Conference on Modelling Fluid Flow (CMFF'25)
The 19th International Conference on Fluid Flow Technologies
Budapest, Hungary, August 26 - August 29, 2025

OPTIMISATION OF INLET GUIDE VANE FOR LARGE AXIAL FANS BASED ON BIG DATA ANALYSIS

Zijian Mao[1,2], Laifa Lu[1,2], Shuiqing Zhou[1,2,3], Weiya Jin[1,2], Zengliang Gao[1,2], Diping Xu[1,2]

[1] College of Mechanical Engineering, Zhejiang University of Technology, Hangzhou 310023,China.
[2] Institue of Innovation Research of Shengzhou and Zhejiang University ofTechnology, Shengzhou 312400,China.
[3]Corresponding Author. College of Mechanical Engineering, Zhejiang University of Technology, Hangzhou 310023,China. E-mail: zsqwh666@163.com

ABSTRACT

Large axial fans are widely used in nuclear power station ventilation systems due to their high flow rate, high total pressure, compact construction, and excellent economic performance under various operating conditions. This paper discusses a large medium-pressure axial fan with a diameter of 1250 mm, a rated air volume of 82,400 m³/h, and a rated air pressure of 2300 Pa. To address complex and variable operating conditions, as well as performance and noise requirements under extreme conditions, a method for optimizing the inlet guide vane (IGV) of the fan based on big data analysis is proposed. The large axial flow fan audio signal is extracted to analyze structural features of non-steady flow, and discrete peak and non-linear frequencies in the frequency domain are obtained. The PANS model based on the v2-f non-linear turbulence model is validated through simulations, with multi-objective optimization using a support vector machine (SVM) and SVM parameter selection optimized using particle swarm optimization (PSO). Results show that with 15 IGVs, an installation angle of 80°, and a distance of 260 mm between the IGV and dynamic vane, a total pressure increase of 187.64 Pa and a noise reduction of 5.32 dB are achieved.

Keywords: Inlet guide vane, Large axial flow fan, Multi-Objective Optimization, PANS model, SVM

NOMENCLATURE

C_p	[-]	Pressure coefficient
D	[m]	Diameter
E	[-]	Mathematical expectation
F	[-]	Sample matrix
L_{ref}	[m]	Reference Lenth
m_1	[-]	Number of IGVs
m_2	[-]	Number of OGVs
n	[*r*/min]	Rotating speed
p	[Pa]	Pressure
p_{tp}	[Pa]	Total pressure
Q	[m³/min]	Volume flow
r	[-]	Failure indicator function
R^2	[-]	Linear regression coefficient
S_i	[-]	Global Sensitivity Indicator
$V(\cdot)$	[-]	Variance Operator
V_{ref}	[m/s]	Reference velocity
x_i	[-]	Random variable
y^+	[-]	A dimensionless parameter
y_l	[-]	Response
Z	[-]	Number of moving blades
z_l	[-]	Random variables
ρ	[kg/m³]	Density
η	[-]	Efficiency
v	[m²/s]	Kinematic viscosity

Subscripts and Superscripts

RSM	Response Surface Model
GERSM	Gradient-Enhanced Response Surface Model
IGV	Inlet guide vane
MSE	Mean Square Error
NSGA-II	Non-dominated Sorting Genetic Algorithm-II
OGV	Outlet Guide Vane
PANS	Partially-Averaged Navier–Stokes
SPL	Sound Pressure Level

1. INTRODUCTION

This study focuses on optimizing the structure of a large nuclear-grade axial fan (1250 mm diameter) used in nuclear power plant ventilation systems, operating at medium pressure (Mach < 0.3, Reynolds > 4000). Optimizing the fan is urgent due to potential risks in the internal flow field that could lead to motor damage, instability, and shutdowns, causing significant economic and social impacts [1,2].

The goal is to increase pressure and reduce noise without increasing fan size, in line with China's carbon neutrality policies [3,4].

Approximate models are often employed to reduce computational costs in fan optimization. For example, CHOI et al. [5] used RSM to improve total pressure and efficiency by 5.2% and 2.0%, TANG et al. [6] applied GERSM to a transonic fan, and NISHI et al. [7] achieved a 9.1% efficiency increase with RSM in a small axial fan.

Unlike previous studies on single-stage blades, this work optimizes a large axial fan by applying global sensitivity analysis to identify key factors for pressure and noise, uses a Kriging model with NSGA-II for optimization, and validates the results with performance and noise tests, offering guidance for other complex fan designs [8,9].

2. NUMERICAL SIMULATION ANALYSIS AND VERIFICATION

2.1. Research objects

Large axial flow fan mainly consists of a fairing, inlet guide vanes, moving blades, outlet guide vanes and a motor, as shown in Figure 1.

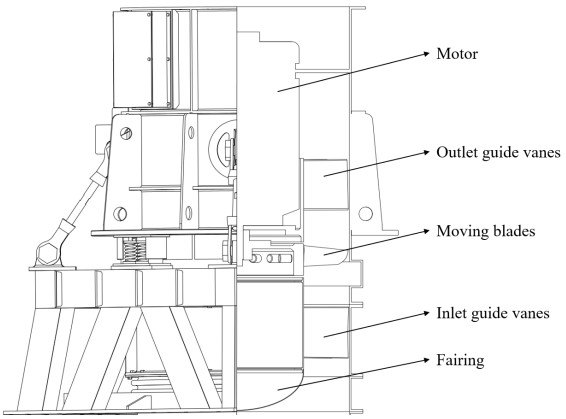

Figure 1 Axial fan structure diagram

2.2. Computational model and verification

For internal area calculations and mesh generation, the fan geometry was divided into five components: inlet, IGV, rotor, OGV, and outlet, as illustrated in Figure 2.

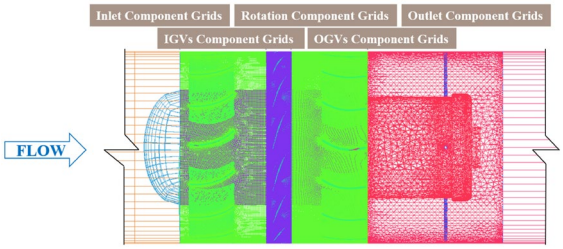

Figure 2. Division of axial fans

Figure 3 shows grid delineation. The important parts (moving vanes, IGVs, OGVs) were structurally meshed to improve the mesh quality. The meshes of IGV, rotation and OGV grids are respectively displayed in Figure 3. In this case, the first node was placed in the region of the viscous substratum with $y^+ \leq 5$. The y^+ empirical formula is expressed as Eq. 1:

$$Y_{wall} = 6\left(\frac{V_{ref}}{\nu}\right)^{-\frac{7}{8}}\left(\frac{L_{ref}}{2}\right)^{\frac{1}{8}} y^+ \qquad (1)$$

where, V_{ref} denotes the reference velocity characteristic of the area-averaged inlet velocity, and L_{ref} represents the reference the fan diameter.

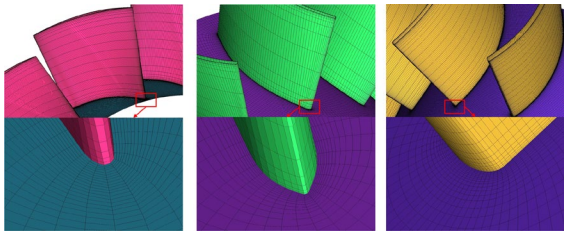

Figure 3. Computational grid of blade

For experimental validation, a C-type air chamber was used according to "GB/T 1236-2017"[10] . The fan was tested at room temperature and pressure, with air parameters recorded using an atmospheric pressure, temperature, and humidity tester at the inlet.

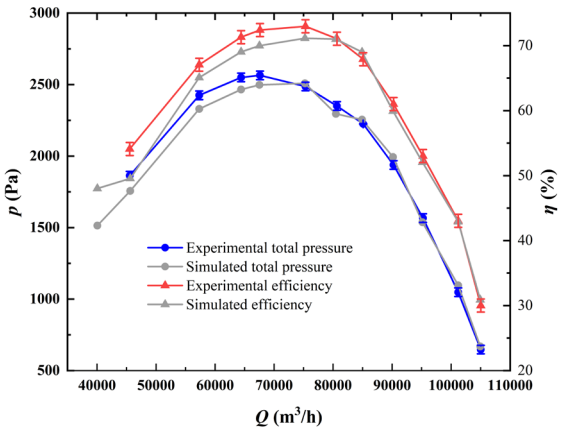

Figure 4. Comparison of experimental and numerical simulation performance curves

Figure 4 compares the numerical simulation with experimental data, showing good agreement. The total pressure simulation was slightly lower, with a maximum error of under 5%. Efficiency differences were minimal, with a maximum error of 9.09% at low flow rates and under 3% at other points, indicating high reliability of the model.

Noise tests followed "GB/T 2888-2008 Fan and Roots Blower Noise Measurement Method,"[11] with the noise receiving point set at 1,250 mm and 45°

horizontally from the outlet center. The schematic of the noise monitoring points and experimental setup is shown in Figure 5(a).

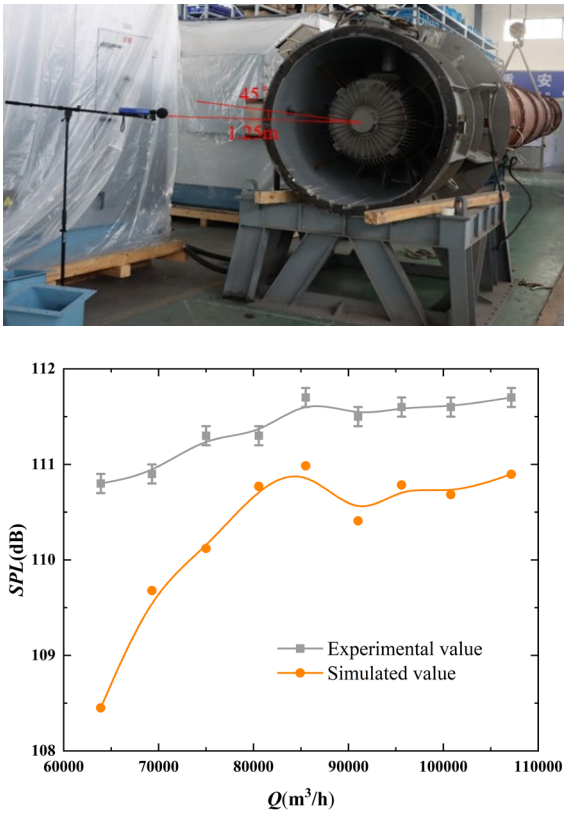

Figure 5. Noise test (a) Noise experimental setup (b) Experimental and numerical simulation noise results

Figure 5(b) shows experimental and simulation noise results. At a flow rate of around 70,000 m³/h, the simulated noise was slightly lower than the experimental value, with a maximum error of under 3%. At flow rates above 75,000 m³/h, the values became more consistent. At the designed flow rate, the average experimental and simulated noise were 111.52 dB and 110.88 dB, respectively, with a relative error of $\leqslant$ 0.57%.

According to JB/T 8690-2014 (Fan Noise Limits)[12], the maximum permissible operational noise level for axial flow fans is 109 dB, and its aerodynamic performance was suboptimal, necessitating optimization. Given the fan's non-standard design and complex structure, analyzing these factors is crucial.

3. DETERMINATION OF OPTIMIZED STRUCTURE

3.1. Global sensitivity analysis method and implementation method

Global sensitivity analys is gives the relationship between the partial derivatives of the output concerning the input variables over the entire input variable space, i.e. $f(\theta)=\partial P_f(\theta)/\partial\theta|_{\theta\in\Theta}$, or a sensitivity indicator used to indicate the importance of the input variables and to rank the importance of the input variables, so it is also known as importance measure analysis.

The global sensitivity metric is defined[13-15] as:

$$S_i=\frac{V[E(I_F\mid x_i)]}{V(I_F)} \tag{2}$$

$$I_F(x)=\begin{cases}1, x\in \text{Invalid Domain}\\ 0, x\notin \text{Invalid Domain}\end{cases} \tag{3}$$

$$V(I_F)=E(I_F^2)-E^2(I_F)=E(I_F)-E^2(I_F) \tag{4}$$

where $V(I_F)$ is the variance operator, $E(I_F\mid x_i)$ is the mathematical expectation of the failure indicator function I_F under the condition of random variable x_i, and I_F is the failure domain indicator function.

For some input variable xi, the global sensitivity principal indicator is:

$$S_i=\frac{V[E(I_F\mid x_i)]}{V(I_F)}=\frac{E(E^2(I_F\mid x_i))-E^2(E^2(I_F\mid x}{E(I_F^2)-E^2(I_F)}=\frac{E(E^2(I_F\mid x_i))-E^2(I_F)}{E(I_F)-E^2(I_F)} \tag{5}$$

The fan mainly consisted of IGV, moving vane, OGV, etc. Therefore, a total of 14 parameters[13], namely the number of IGV ω_1, the number of moving vane ω_2, the number of OGV ω_3, hub ratio ω_4, IGV and moving vane spacing ω_5, moving vane and OGV spacing ω_6, blade top clearance ω_7, IGV bending angle ω_8, IGV chord length ω_9, moving vane bending angle ω_{10}, moving vane swept angle ω_{11}, OGV bending angle ω_{12}, OGV chord length ω_{13}, fan diameter ω_{14}, were analyzed by the Sobol' global sensitivity analysis method. The analysis procedure is specifically displayed in Figure 6 and the schematic diagram of structural parameters is shown in Figure 7.

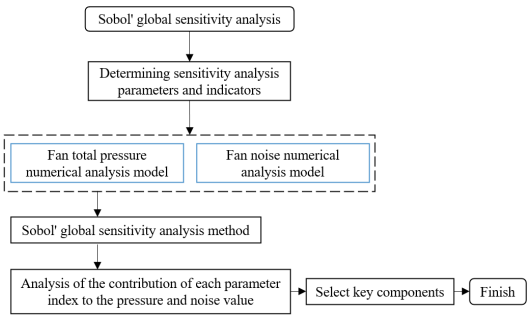

Figure 6. Flow chart of sensitivity analysis

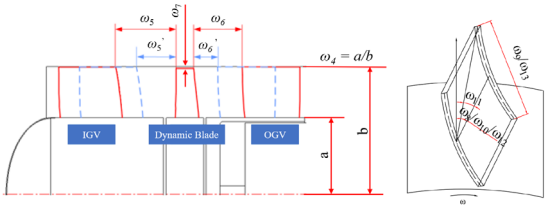

Figure 7. Structural parameters

The global sensitivity values of each parameter to the total pressure and noise of the fan were obtained, as illustrated in Figure 7. In general, the influence of parameters such as IGV bend angle ω_8, IGV and moving vane spacing ω_5, and IGV chord length ω_9 was greater, among which moving vane bend angle ω_{10} and IGV bend angle ω_8 had the highest total global sensitivity values to pressure, which were 31.214 % and 30.113 %, respectively, and IGV bend angle ω_8 and IGV and moving vane spacing ω_5 had the highest total global sensitivity values to noise, which were 33.124 % and 30.145 %, respectively.

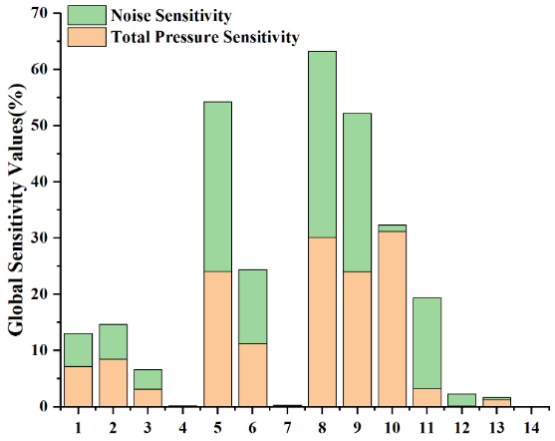

Figure 8. Summary of global sensitivity

According to the above analysis, IGV and moving vane had a large impact while OGV had a relatively small impact on the aerodynamic performance and noise. The internal flow characteristics of the fan will be analyzed as follows to further clarify the optimization objective.

3.2. Analysis of the internal flow characteristics of the fan

The radial section of the hub with blade flow surface R = 280 mm (0.5 times the blade height, Plane1) was selected to study the internal flow characteristics of the fan, and a vertical section was made over the center of the fan circle (as shown in Plane 2). Figure 9 shows the schematic diagram of the radial section of the hub.

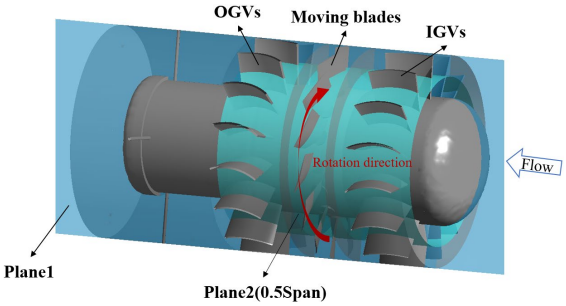

Figure 9. Internal structure of the fan

Figure 10 shows the velocity vector distribution on Plane 1. There was an obvious vortex in the IGV area, which was located between the IGVs. The vortex was mainly concentrated on the pressure surface of the IGV, which was attributable to the blade shape of the guide vane. At the same time, there was a low-speed region in the reflux area, while a high-speed region on the suction surface of the moving blade, which resulted in flow disorder in the dynamic-static coupling zone between the IGV and the moving vane.

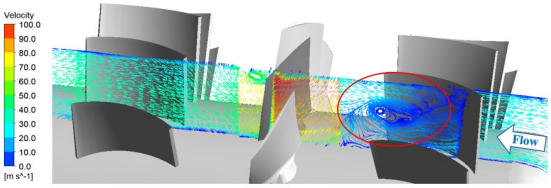

Figure 10. The velocity vector distribution

As a part of the fan, IGV deflected the air flow before entering the hub, increased the flow rate and pressure drop. It was hence an important part of a large axial flow fan. The above analysis also indicates that the structural design of the IGV was not rational and had a significant impact on the performance and noise of the fan, so IGV was identified as the optimization objective of this study.

4. KRIGING MULTI-OBJECTIVE OPTIMIZATION

4.1. Parameterization

The parameters of the IGV are shown in Figure 11. The IGV midline was determined by chord length σ_a, angle α corresponding to the chord, tip deflection angle was defined as β, and the axial distance from the nearest point of the IGV midline to the leading edge of the moving vane as σ_b. These four parameters were optimized in this study.

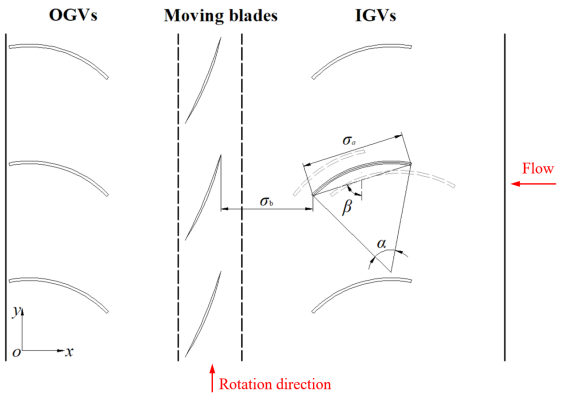

Figure 11. Structure parameters of IGVs

A single circular arc blade is generally adopted in the nuclear power fans. The new IGV midline can be obtained by controlling parameter change and characterizing profile change. Under the premise of ensuring the smooth curvature of the blade, the variable range of each parameter is determined as follows: σ_a: 234~350 mm, α: 44~68 °, β: 58~86 °, σ_b: 208~312 mm.

4.2. Kriging model and optimization

This study and [13] share similar test rigs and parameter ranges, but here we introduce a big data-driven optimization workflow and broader sensitivity analysis, making the results more robust and widely applicable.

Kriging model is an unbiased estimator with minimum variance. The design variables $x_i \in X = [x_1, x_2, \cdots, x_n]^T$ and response values $y_l \in Y = [y_1, y_2, \cdots, y_n]^T$ were assumed to follow a standard normal distribution. The unbiased estimation y_l^* of the random inputs x_l corresponding to y_l is shown as:

$$y_l^* = f(x)^T \beta + z_l(x), \quad l = 1, 2, \cdots, q \tag{6}$$

$$\beta = \left(F^T R^{-1} F\right)^{-1} F^T R^{-1} Y \tag{7}$$

$$\gamma^* = \frac{z_l(x)}{r(x)^T} = R^{-1}(Y - F\beta) \tag{8}$$

To establish the Kriging model, samples should be obtained through experimental design. The optimal Latin hypercube experiment design (Opt LHD) is generally adopted to overcome the deficiencies of random sample space selection and sample concentration in Latin hypercube method. And its formula is expressed as:

$$G_{(L)} = \sum_{i=1}^{N} \sum_{j=i+1}^{N} \frac{1}{\left\| x_i - x_j \right\|^2} \tag{9}$$

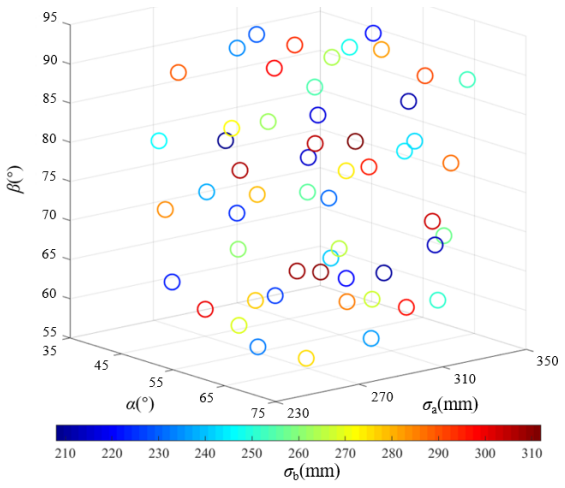

Figure 12. Spatial distribution of samples

As shown in Figure 12, 55 spatial samples were generated using the overshoot method, with the first 50 used to draw IGV profiles. The samples are evenly distributed in the design space. The design variables are IGV chord length (σa), rounding angle (α), tip deflection angle (β), and shortest axial distance (σb), with total pressure and noise as optimization objectives. The mathematical model is as follows:

$$\begin{cases} Max\left(P(\sigma_a, \alpha, \beta, \alpha_b)\right) \\ Min\left(SPL(\sigma_a, \alpha, \beta, \alpha_b)\right) \\ s.t. \quad 234 \le \sigma_a \le 350 \\ 44 \le \alpha \le 68 \\ 57 \le \beta \le 86 \\ 208 \le \alpha_b \le 312 \end{cases} \tag{10}$$

The constraint is:

$$\begin{cases} Q = 82400 \\ SPL \le 111.7 \end{cases} \tag{11}$$

$$MSE = \sum_{i=1}^{n} \frac{1}{n} (f(x_i) - y_i)^2 \tag{12}$$

$$R^2 = 1 - \frac{\sum_{i=1}^{n} (y_i - \hat{y}_i)^2}{\sum_{i=1}^{n} (y_i - \bar{y})^2} \tag{13}$$

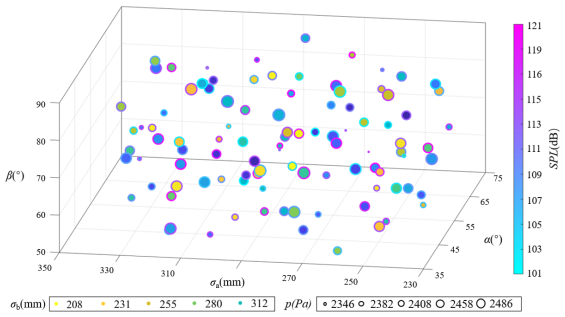

Figure 13. Kriging model fitting results of design variables and total pressure and SPL

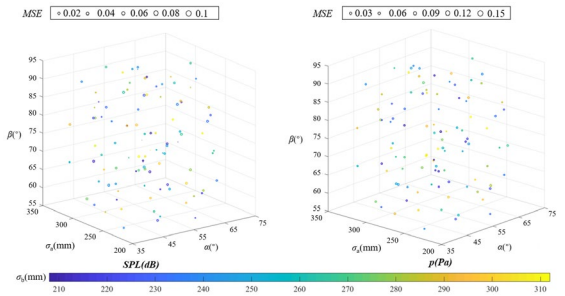

Figure 14. Fitted mean square error MSE

Figures 13 and 14 show the Kriging model fitting results and MSE, with values below 0.1 for noise and 0.15 for pressure, indicating good accuracy. NSGA-II was used for optimization, with optimal results in Table 2. Table 3 shows further reduced MSEs, confirming the effectiveness of the multi-objective optimization.

Table 2. Comparison of parameters before and after optimization

	σ_a (mm)	α (°)	β (°)	σ_b (mm)
Original	292	56	72	260
Optimization	298	61	76	310

Table 3. MSE before and after optimization

	Variable	MSE
Original	*SPL*	0.0434
	p	0.0895
Optimization	*SPL*	0.0235
	p	0.0338

4.3. Optimization result and model

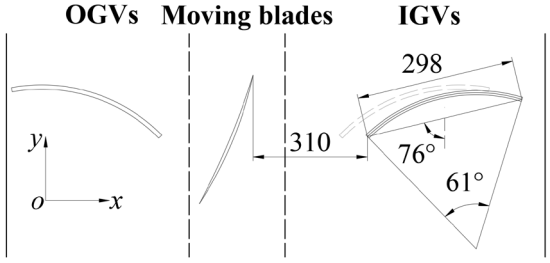

Figure 15. Settings optimization model structure

Fig. 15 shows the settings optimization of IGV. The chord length σ_a of the IGV was increased by 55 mm, the corresponding circular angle α by 5°, the nearest distance σ_b from the IGV to the moving vane by 48 mm, and its angle with the y-axis β by 3°. The physical models are compared in Figure 16.

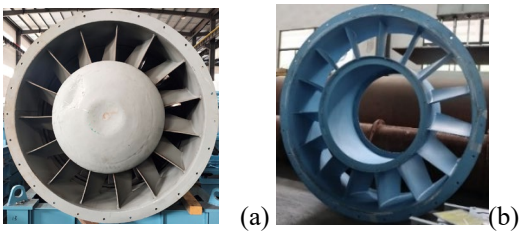

Figure 16. Comparison models (a) Original model (b) Optimization model

5. COMPARISON BEFORE AND AFTER OPTIMIZATION

5.1. Simulation result before and after optimization

To study the internal flow characteristics of the optimized fan, three planes were intercepted in the hub radial direction along the blade height located at R=150 mm (10% blade height), R = 280 mm (50 % blade height) and R = 430 mm (90 % blade height) in the hub radial direction. The rotary surface is shown in Figure 17.

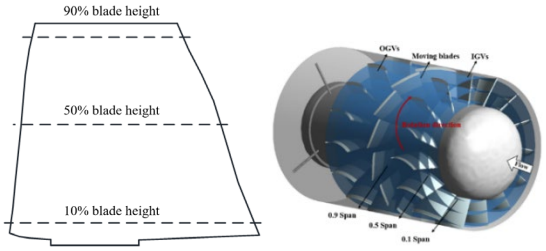

Figure 17. Schematic diagram of the rotating surface

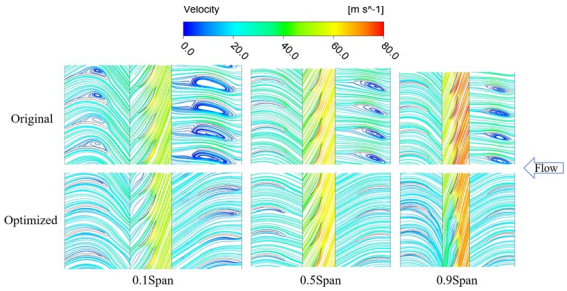

Figure 18. Streamlines coloured by flow velocity at different spans

Figure 18 compares IGV streamlines before and after optimization, showing that vortices present at all heights were eliminated, leaving only low-speed zones. Figure 19 displays simulated static pressure distributions at IGV heights, with Cp calculated using Eq. 13 [16,17].

$$C_p = \frac{p - p_\infty}{\frac{1}{2}\rho_\infty v_\infty^2} \tag{14}$$

Figure 20 shows static pressure distributions. After optimization, Cp increased, pressure gradients decreased, and the separation point shifted, leading to smoother pressure and fewer vortices, thus reducing noise.

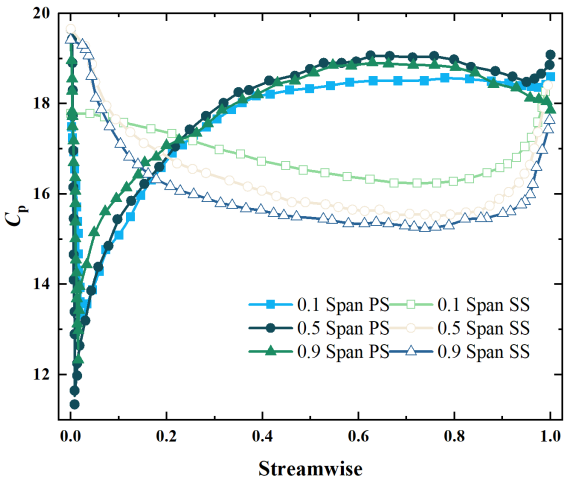

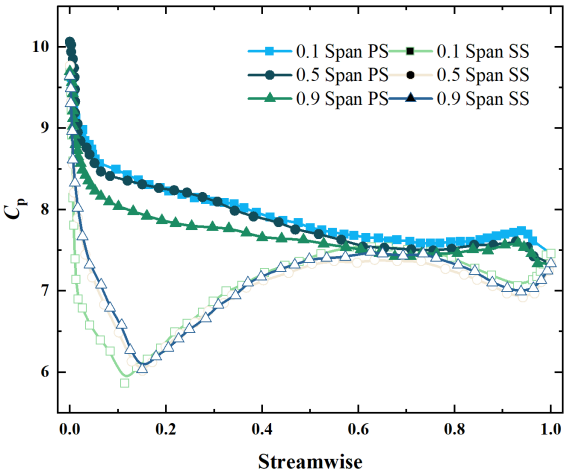

Figure 20. IGVs pressure distribution (a) Original (b) Optimization

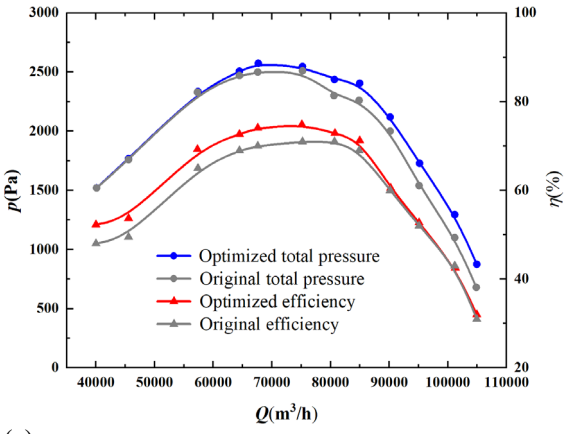

(a)

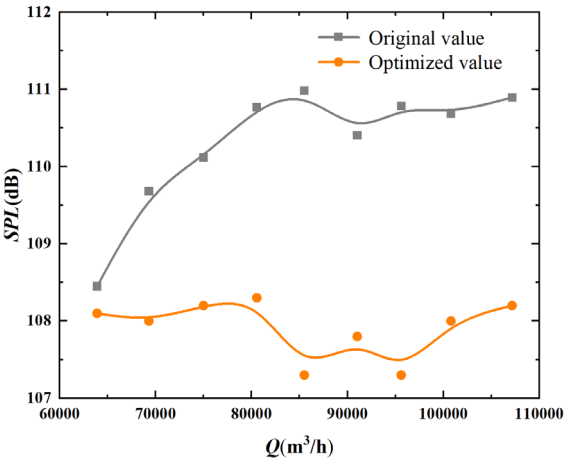

(b)

Figure 21. Numerical simulation results of aerodynamic performance (a) *Q* (b) SPL

Figure 21 shows the numerical simulation results before and after optimization. After optimization, total pressure and efficiency improved at all flow rates. Total pressure increased by 140.97 Pa at flow rates above 70,000 m³/h, while efficiency improved by 2.06% at flow rates below 85,000 m³/h, as shown in Figure 21(a). Noise was reduced by 3.08 dB at all flow rates at the design condition, as shown in Figure 21(b).

5.2. Experimental result before and after optimization

Figure 22 shows the total pressure and efficiency curves for the original and optimized fans across the full range of flow rates. At the design operating point (82,400 m³/h), the optimized model achieves a total pressure increase of 156.4 Pa and an efficiency improvement of 0.86% compared to the original design. All values are area-averaged outlet measurements based on the GB/T 1236-2017 standard. Minor differences between plotted and tabulated values are due to sampling and measurement uncertainty.

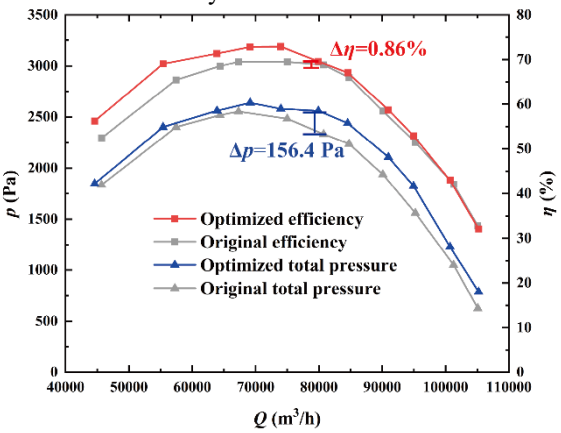

Figure 22. Comparison of performance curves

Referring to the noise test standard, noise receiving points were set at 45 ° from the center of the outlet surface, one time that of the diameter at a horizontal position, and the noise of the optimized fan was also tested.

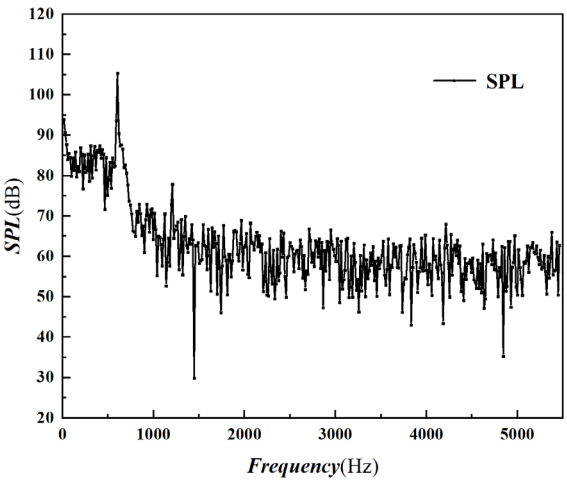

Figure 23. Comparison of noise spectrum

Figure 23 compares the far-field SPL spectra of the original and optimized fans at 82,400 m³/h. Both

show peaks at 14, 302, and 604 Hz. After optimization, the fundamental frequency peak drops from 111.7 dB to 105.3 dB, indicating reduced discrete noise.

6. CONCLUSIONS

This study conducted multi-objective optimization of an IGV for a large axial fan using NSGA-II, validated through experiments and simulations.

(1) Sobol' global sensitivity analysis showed that the IGV bending angle and moving blade bending angle are most sensitive to total pressure, while the distance between the IGV and moving blade affects noise the most. Internal flow analysis revealed significant vortex formation between IGVs, concentrated on the pressure surface.

(2) Numerical simulations of IGV pressure distribution showed smoother static pressure gradients and reduced vortex shedding post-optimization. Experimental results confirmed improved fan performance, with a total pressure increase of 156.4 Pa, a 0.85% efficiency gain, and a 6.4 dB noise reduction.

(3) The NSGA-II optimized Kriging model proved effective for multi-objective IGV design and provides new ideas for optimizing large axial fans.

REFERENCES

[1] Zhao, F.T., Jing, X.D., Yang, M.S., Wang, D.Y., Sha, Y.D., and Luan, X.C. (2020). Experimental study of rotor blades vibration and noise in multistage high pressure compressor and their relevance. Chinese Journal of Aeronautics 33(3), 870-878.

[2] Gu, Z.Y., Zhu, Y.Y., Xiang, J.L., and Zeng, Y. (2021). A prediction method of operation trend for large axial-flow fan based on vibration-electric information fusion. Journal of Central South University 28(6), 1786-1796.

[3] Zhang, W.J., Yuan, J.P., Zhou, B.L., Li, H., and Yuan, Y. (2018). The influence of axial-flow fan trailing edge structure on internal flow. Advances in Mechanical Engineering 10(11).

[4] Fakhraei, A., Faghihi, F., Rabiee, A., and Safarinia, M. (2021). Coolant flow rate instability during extended station blackout accident. Progress in Nuclear Energy 131.

[5] Zhang, C., Li, A.G., Li, J.X., Hou, Y.C., and Chen, X. (2021a). Radiation noise control of a 90 degrees rectangular elbow in ventilation and air conditioning systems. Journal of Building Engineering 37.

[6] Hu, Z.H., and Lu, W. (2017). "Numerical Investigation on Performance and Aerodynamic Noise of High Speed Axial Flow Fans", IAEAC, 885-889.

[7] Kromer, F.J., Moreau, S., and Becker, S. (2019). Experimental investigation of the interplay between the sound field and the flow field in skewed low-pressure axial fans. Journal of Sound and Vibration 442, 220-236.

[8] Tanasic, N., Jankes, G., and Skistad, H. (2011). Cfd analysis and airflow measurements to approach large industrial halls energy efficiency: A case study of a cardboard mill hall. Energy and Buildings 43(6), 1200-1206.

[9] Choi, Y.S., Kim, Y.I., Kim, S., Lee, S.G., Yang, H.M., Lee, K.Y., et al. (Year). "A Study On Improvement Of Aerodynamic Performance For 100hp Axial Fan Blade And Guide Vane Using Response Surface Method", in: ASME-JSME-KSME Joint Fluids Engineering Conference (AJK-FED 2019)).

[10] GB/T 1236-2017(2017). Standardized Air Duct Performance Test for Industrial Ventilators. Beijing: China Standard Press.

[11] GB/T 2888-2008(2008). Methods of noise measurement for fans blowers compressors and roots blowers. Beijing: China Standard Press.

[12] JB/T 8690-2014 (2014). Fans Noise Limited value. Beijing: China Standard Press.

[13] Tang, X., Luo, J.Q., and Liu, F. (2017). Aerodynamic shape optimization of a transonic fan by an adjoint-response surface method. Aerospace Science and Technology 68, 26-36.

[14] Nishi, Y., Mori, N., Yamada, N., and Inagaki, T. (2022). Study on the design method for axial flow runner that combines design of experiments, response surface method, and optimization method to one-dimensional design method. Renewable Energy 185, 96-110.

[15] Venturelli, G., and Benini, E. (2016). Kriging-assisted design optimization of S-shape supersonic compressor cascades. Aerospace Science and Technology 58, 275-297.

[16] Zhou, S.Q., Hu, Y.J., Lu, L.F., Yang, K., and Gao, Z.L. (2022). IGV Optimization for a Large Axial Flow Fan Based on MRGP Model and Sobol' Method. Frontiers in Energy Research 10.

[17] Cui, L.J., Lu, Z.Z., and Zhao, X.P. (2010). Moment-independent importance measure of basic random variable and its probability density evolution solution. Science China-Technological Sciences 53(4), 1138-1145.